

Light correcting light with nonlinear optics

Sachleen Singh¹, Bereneice Sephton^{2,3,*}, Wagner Tavares Bueno¹, Vincenzo D'Ambrosio², Thomas Konrad³ and Andrew Forbes¹

¹University of the Witwatersrand, School of Physics, Johannesburg, South Africa

²Università degli studi di Napoli "Federico II", Dipartimento di Fisica "E. Pancini", Napoli, Italy

³University of KwaZulu-Natal, School of Chemistry and Physics, Durban, South Africa

Abstract. Structured light, where complex optical fields are tailored in all their degrees of freedom, has become highly topical of late, advanced by a sophisticated toolkit comprising both linear and nonlinear optics. Removing undesired structure from light is far less developed, leveraging mostly on inverting the distortion, e.g., with adaptive optics or the inverse transmission matrix of a complex channel, both requiring that the distortion be fully characterized through appropriate measurement. We show that distortions in spatially structured light can be corrected through difference-frequency generation in a nonlinear crystal without any need for the distortion to be known. We demonstrate the versatility of our approach using a wide range of aberrations and structured light modes, including higher-order orbital angular momentum (OAM) beams, showing excellent recovery of the original undistorted field. To highlight the efficacy of this process, we deploy the system in a prepare-and-measure communications link with OAM, showing minimal cross talk even when the transmission channel is highly aberrated, and outline how the approach could be extended to alternative experimental modalities and nonlinear processes. Our demonstration of light-correcting light without the need for measurement opens an approach to measurement-free error correction for classical and quantum structured light, with direct applications in imaging, sensing, and communication.

Keywords: phase conjugation; aberration correction; orbital angular momentum; nonlinear optics.

Received Nov. 30, 2023; revised manuscript received Jan. 15, 2024; accepted for publication Jan. 19, 2024; published online Feb. 28, 2024.

© The Authors. Published by SPIE and CLP under a Creative Commons Attribution 4.0 International License. Distribution or reproduction of this work in whole or in part requires full attribution of the original publication, including its DOI.

[DOI: [10.1117/1.AP.6.2.026003](https://doi.org/10.1117/1.AP.6.2.026003)]

1 Introduction

Light, and with it, the transverse tailoring of phase and amplitude to create so-called structured light,^{1,2} presents a large field of active research with wide-ranging applications,³ from optical trapping⁴ to communication.⁵ The toolkit has become highly versatile covering generation, control, and detection schemes that include liquid crystals,^{6,7} digital micromirror devices,⁸ and metasurfaces.^{9,10} Beyond linear optics, structured light control with nonlinear optics has become topical of late,¹¹ shifting the focus of attention from wavelength change and efficiency to spatial modal creation, control, and detection. This has led to a reinvention of the field with a modern twist, ushering in new selection rules^{12–14} and processes^{15–18} while fostering wide-reaching applications, including spatial mode creation^{19–21} and

detection,^{22,23} image processing^{24–27} and filtering,²⁸ holography,^{29–31} enhanced interferometry,³² high-dimensional teleportation,^{33,34} as well as the development of modern nonlinear materials.^{35–38}

Unfortunately, the spatial structure of light becomes distorted in complex channels,^{39–42} arresting its full potential. Although phase conjugation of structured light is possible by nonlinear optics,⁴³ it does not correct the distortion but rather produces the negative of it, requiring a time reversal step.⁴⁴ To mitigate these drawbacks, a measurement-based approach to structured light correction is now ubiquitous, for example, using adaptive optics^{45–49} and wavefront shaping,⁵⁰ inversion of the transmission matrix of complex channels,^{51–53} and finding invariances that remain distortion-free.^{54–56}

Here we show that light can correct light without the need for any measurement. We exploit parametric wave mixing by difference-frequency generation (DFG) in a nonlinear crystal (NLC) to restore the information encoded into the structure of light,

*Address all correspondence to Bereneice Sephton, bereneice21@gmail.com

[†]These authors equally contributed to this work.

even after it has passed through a highly aberrating channel. In order to achieve this, two input beams, one with information encoded into its structure and the other as a probe, are passed through the same aberrating channel followed by DFG in an NLC, returning only the desired information. This is due to the nature of the parametric wave-mixing process, which outputs the product of one of the input modes with the conjugate of the other. We demonstrate the versatility of our approach using a wide range of aberrations and structured light modes, from Gaussian beams to orbital angular momentum (OAM) beams and their superpositions and show excellent recovery of the original undistorted field. To highlight the efficacy of this, we consider the cross talk matrix of a 15-dimensional OAM alphabet across a noisy channel comprising an arbitrary aberration, showing very good recovery of the information. We outline how our approach can be used across multiple wavelengths that could be close or far apart, offering an approach to measurement-free error correction for classical and quantum structured light.

2 Materials and Methods

2.1 Concept

With DFG, two electric fields (E_1 and E_2) mix in a second-order NLC to generate a third beam (E_G). Here each field possesses a transverse spatial structure $M_n(r, \phi)$ and polarization, indicated by the unit vector \hat{e}_n ,

$$E_n = M_n(r, \phi)\hat{e}_n, \quad (1)$$

where $n = \{1, 2, G\}$ refers to the first, second, and generated beams, whereas (r, ϕ) are the radial and azimuthal coordinates in the transverse spatial plane. Coherent amplification of the generated field occurs along the crystal length when the phase-matching conditions are satisfied. This applies a constraint between the wave vectors and interacting fields,⁵⁷ ensuring conservation of energy and momentum in the process. For DFG, the energy of the generated field in the paraxial regime is aptly given by the difference of the input angular frequencies, $\omega_1 - \omega_2 = \omega_G$ and wave vectors, $\mathbf{k}_1 - \mathbf{k}_2 = \mathbf{k}_G$ for the transverse components of the interacting fields. A sufficiently large bandwidth for phase matching of the longitudinal component in the thin-crystal limit causes the spatial profile of the generated field to be reduced to the product of the two input fields.⁵⁸ Following from the conservation rules, the output field then holds the combined information of the input fields such that the spatial structure of the generated field is proportional to that of the first input and the complex conjugate of the second input,

$$M_G = \eta M_1 M_2^*, \quad (2)$$

where η is a constant related to the efficiency of the process and * indicates complex conjugation.

By considering the complex form of the spatial structures at the beam waist (neglecting propagation terms for simplicity), $M_n = A_n(r, \phi)e^{i\Phi_n(r, \phi)}$, where $A(r, \phi)$ is the amplitude and $\Phi(r, \phi)$ the phase, the effect of DFG is to conjugate the phase distribution of the second beam and add it to the phase distribution of the first, $\Phi_G = \Phi_1 + (-\Phi_2)$. Where the second beam's phase is uniform or null, the generated beam phase is simply that which is carried by the first ($\Phi_G = \Phi_1$). As a result, the generated beam will contain any desired structure (Φ_{info})

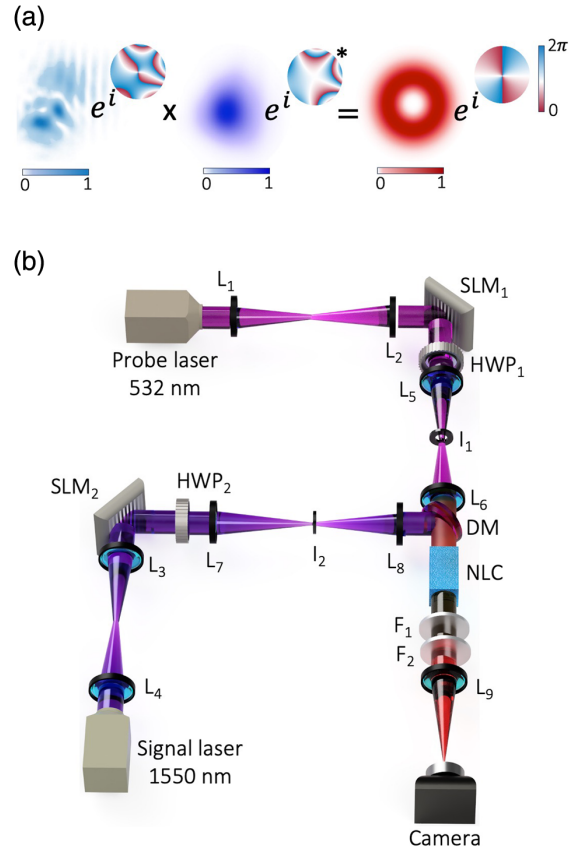


Fig. 1 (a) Concept of correcting aberrated states by using light to correct light. The product of an input beam (middle mode) with another containing the same phase aberration (exponential term) cancels the identical distortion present in the structure carried by a second input beam (left mode) to restore the unaberrated state (right mode) in the difference-frequency beam generated from nonlinear wave mixing. Beams are shown in the far field for conceptual clarity. (b) Experimental setup used to apply and correct distortions on structured modes with DFG. SLM, spatial light modulator; HWP, half-wave plate; I, aperture; DM, dichroic mirror; NLC, nonlinear crystal; F₁, short-pass and F₂ long-pass wavelength filters; and L₁ (18 mm), L₂ (200 mm), L₃ (300 mm), L₄ (75 mm), L₅ (500 mm), L₆ (100 mm), L₇ (750 mm), and L₈ (100 mm) are lenses.

that the first beam contains. This, however, is true for any additional distortions (Φ_{Ab}) experienced by the beam as well. For such an event, the generated beam will then have a phase of $\Phi_G = \Phi_{\text{info}} + \Phi_{\text{Ab}}$, such that the modal information or purity is degraded and seen in distortion of the intensity profile upon propagation. One may now consider the case where the contribution of the second beam can be exploited. Without loss of generality, we consider an example where we seek to restore Laguerre–Gaussian (LG _{ℓ}) modes of zero radial index ($p = 0$) and arbitrary ℓ , from an aberrated state. Figure 1(a) illustrates this concept. Notably, these structured modes hold OAM as a degree of freedom and are characterized by the integer parameter ℓ , which yields $\ell\hbar$ OAM per photon and ℓ number of twists in the phase front per wavelength (red to blue transitions in the rightmost phase inset). To correct the aberration, one need only see that by using the same aberration phase on the second beam, the original helical phase can be restored. The distortion of the

LG mode amplitude (depicted alongside the phase terms) is then corrected to reveal the characteristic doughnut intensity distribution. Here, due to the naturally occurring phase conjugation in the crystal, the initial disturbance, e.g., $M_1 = \text{LG}_{(\ell=2)} e^{i\Phi_{\text{Ab}}}$, also present in the second beam (using a Gaussian profile to conserve the structure of the first beam), e.g., $M_2 = \text{LG}_{(\ell=0)} e^{i\Phi_{\text{Ab}}}$, cancels the distortion in the generated beam, $\Phi_G = (\Phi_{\text{info}} + \Phi_{\text{Ab}}) - \Phi_{\text{Ab}} = \Phi_{\text{info}}$, while preserving the initial phase and amplitude. Cancellation of the unwanted disturbance, such as turbulence, and successful transfer of the desired structure carried by the first beam is therefore achieved using the structure of one light beam to correct that of the other. Note that while we have outlined the concept with second-order nonlinear processes (χ^2), the core principle holds for parametric wave-mixing processes of even order (χ^{2n}) in higher-order difference wave mixing too, or even with cascaded crystals for better wavelength selection (see Appendix).

2.2 Experimental Implementation

To demonstrate the principle of using a second beam in DFG to correct phase aberrations on an initial input beam, we implemented the experimental setup, as shown in Fig. 1(b). Here, two continuous wave lasers of wavelengths 532 nm (VIS) and 1550 nm (IR) were collimated and expanded onto liquid crystal spatial light modulators (SLM₁, SLM₂), before demagnification and imaging onto a type-0 NLC (periodically poled KTP) with a 4*f*-lens system (L₅, L₆ and L₇, L₈). Complex amplitude modulation⁵⁹ was used to encode the desired states of each input beam, which we will refer to as probe and signal beams to clarify their roles in the correction process. Apertures (I₁, I₂) in the Fourier plane spatially filtered the first-order modulated light from the SLMs, respectively, forming the signal and probe input modes. Half-wave plates (HWP₁, HWP₂) in each arm then, respectively, adjusted the polarization for phase matching and a dichroic mirror (DM) was used to collinearly combine the beams before the NLC. A long- and a short-pass wavelength filters (F₁, F₂) placed after the crystal isolated the DFG beam. The generated beam was then focused onto a camera by a lens in a 2*f* configuration (F₉), detecting the Fourier plane of the DFG modes. Here we choose to observe the far-field intensity as the phase-to-amplitude coupling allows us to clearly discern the presence of aberration, highlighting the fact that the aberrations never need be known.

3 Results

We now experimentally realize this concept with the results shown in Fig. 2. Here, three azimuthally varying phase aberrations, $\Phi_{\text{Ab}} = \exp(i\pi \cos(n\phi))$, where $n = \{1, 2, 3\}$ (shown in the top insets) were applied to the IR Gaussian signal beam. The Gaussian structure and flat phase of the IR probe beam are retained for the process. As expected, aberrations on the generated mode distort the beams in the far field, as seen in the top row. By employing the light-correcting light approach with DFG, implemented by now applying the same aberrational phase to the VIS probe beam, we find the initial structure is corrected and confirmed with unaberrated Gaussian distributions in the bottom row.

In Fig. 3, we next explore aberrations having both radial and azimuthal dependence, while also expanding the encoded states to higher-order modes. We note any spatial modes may be used and chose LG due to their extensive applications from

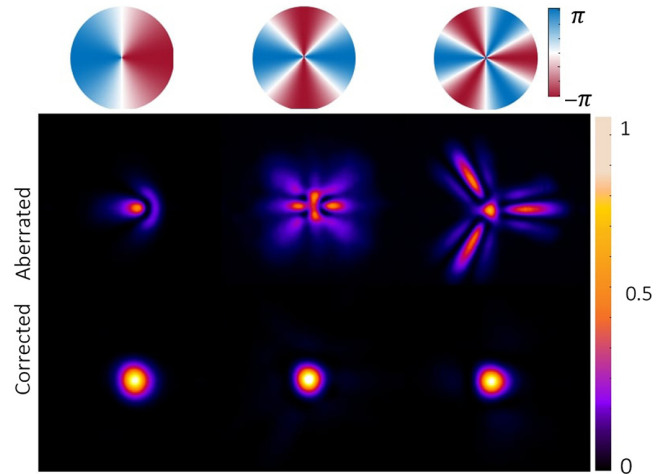


Fig. 2 Three azimuthal aberrations (top insets) were applied to a Gaussian signal beam, resulting in measured intensity distortions in the far field (aberrated row). Application of the nonlinear correction process with a probe beam results in the recovery of the initial Gaussian beam, as evident in the measured far-field intensities in the bottom row (corrected). All intensities are normalized to 1.

communications to metrology.^{60,61} The Zernike basis ($Z_{m,n}$)⁶² with azimuthal frequency, n , and radial order, m , is used to simulate the unwanted distortions, forming a natural basis for optical aberrations.^{63,64} Modes representing astigmatism ($Z_{2,2}, Z_{2,-2}$) and trefoil ($Z_{3,3}, Z_{3,-3}$) were then chosen from the Zernike family and applied with the same strength (i.e., the beams have the same phase gradient and periodicity at each overlapping point). The expected doughnut intensity distributions of these LG states (first three panels) show good agreement with the unaberrated DFG intensities (NA, top right of each modal set). After the structured signal beam encounters each aberration, however, significant deviations in the DFG intensity profiles (Ab.) are observed, obscuring the modes and related information. Applying the same phase distortion to the Gaussian probe shows successful restoration of the modal structure in the DFG beam by cancellation of the aberrational phase (Cor.). Applicability to states with more modal complexity is further demonstrated by constructing modes from a superposition of LG states [$\frac{1}{\sqrt{2}}(\text{LG}_\ell + \text{LG}_{-\ell})$], giving 0 to π wedge phase steps with petal intensity structures. This is shown in the last two panels, where $\ell = \{2, 3\}$, respectively. Similarly, aberrations caused notable distortions in the detected intensity distributions but excellent restoration when applying our correction approach.

Greater aberrational complexity is also introduced by taking three, $\Phi_{\text{Ab}} = 5Z_{2,2} + 5Z_{2,-2} + 10Z_{3,3}$, and four, $\Phi_{\text{Ab}} = 10Z_{2,2} - 10Z_{2,-2} - 10Z_{3,3} + 10Z_{3,-3}$, mode superpositions of the Zernike basis states. This is shown in Figs. 4(a) and 4(b), respectively, where the signal beam was also encoded with LG modes of $\ell \in [1, 6]$. Here deleterious distortions obscure the encoded doughnuts (top insets) into intermittent linear structures (bottom rows, Ab.). With the same phase distortion on the probe beam, we again find the output structure returns to the ring profile. While the modes are excellently restored, a reduction in the correction efficacy appears as the ℓ value increases. This can be attributed to an increase in the generated beam size of $w_\ell = w_0 \sqrt{(|\ell| + 1)}$,

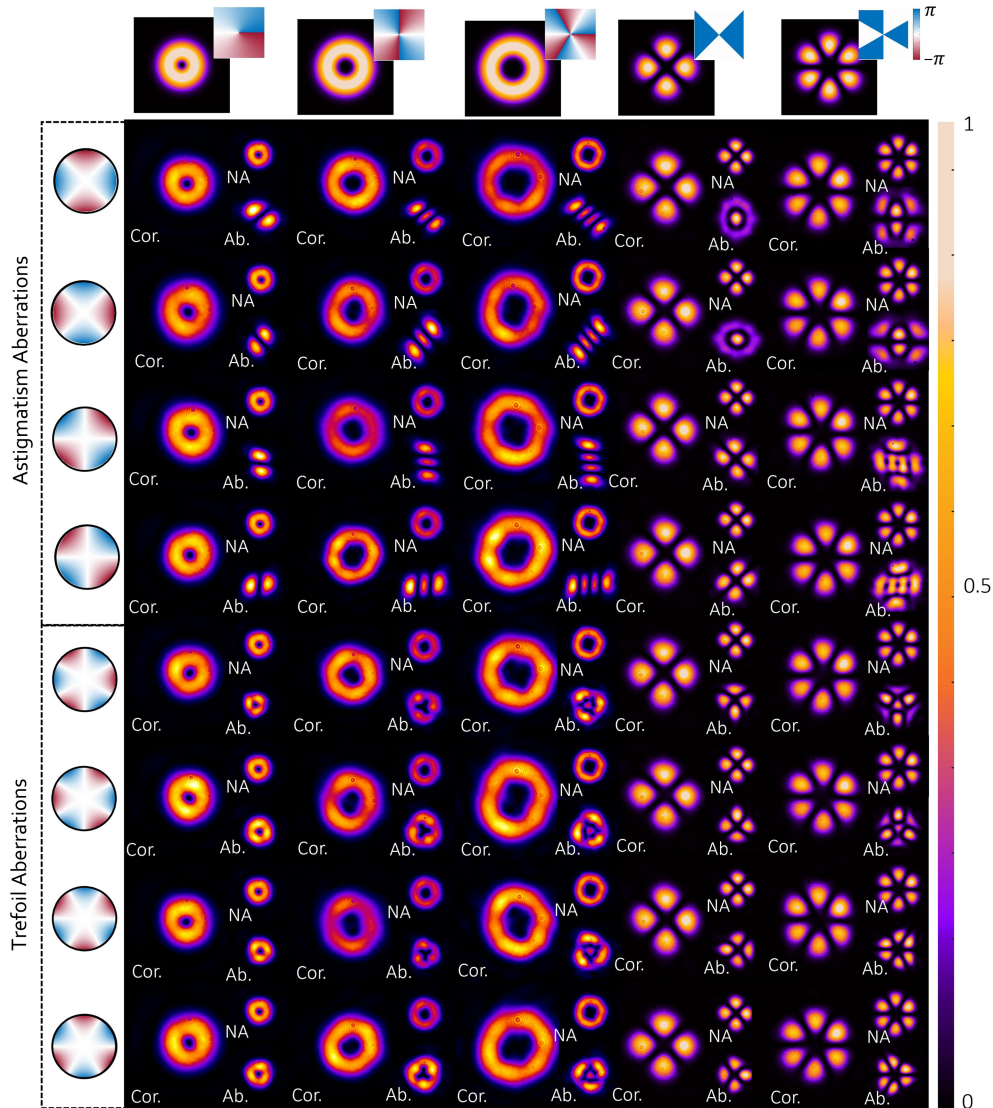


Fig. 3 Experimental correction of astigmatism and trefoil aberrations for five different spatial states (column-wise), where $\ell = \{1, 2, 3\}$, and petal modes with LG superpositions ($\frac{1}{\sqrt{2}}(\text{LG}_\ell + \text{LG}_{-\ell})$), where $\ell = \{2, 3\}$. The correction has been applied for both vertical and oblique combinations of aberrations. Further, every such combination has been corrected for both positive and negative strength coefficients. The applied phase distortion has been shown in the left panel. Every experimental picture shows results for corrected (Cor.) mode with corresponding aberrated (Ab.) and not aberrated (NA) modes as insets. The expected simulated intensity and phase profiles have been shown in the top row.

where w_ℓ is the OAM beam waist and w_0 is the waist of the fundamental Gaussian mode. As a result of increasing size, greater interaction with the optical elements occurs, leading to the modes obtaining additional peripheral aberrations not encoded and accounted for in the probe profile. In Fig. 4(c), the same four-mode aberration is applied to the previous petal superpositions, where $\ell \in [1, 6]$. The aberrating phases on the signal beam similarly destroy the DFG structure, such that they can no longer be identified in comparison to the expected distributions [top insets in Fig. 4(c)]. Excellent agreement then occurs when the probe is used to correct for the distortion. While a small decrease in correction efficacy is also seen as ℓ increases, favorable restoration is still seen up to the largest state.

We now consider the practical application of our concept where the aberrating medium is dispersive. In such a case, the phase accumulation for the two wavelengths will differ by a factor $\alpha = \frac{\varphi_{\lambda_2}}{\varphi_{\lambda_1}} = \frac{\lambda_1 n_{\lambda_2}}{\lambda_2 n_{\lambda_1}}$, a constant value that is fixed by the chosen wavelengths. Accordingly, one need only account for a difference in the strength for the same aberrational distribution. This is easily addressed by our scheme, as shown by two approaches in Fig. 5. In Fig. 5(a), resizing one beam relative to the other, after undergoing distortion, achieves a change in the respective aberrational strength overlapping with the unsized beam. Intuitively, such resizing alters the phase gradient seen by the other beam and so can be used to perfectly correct for

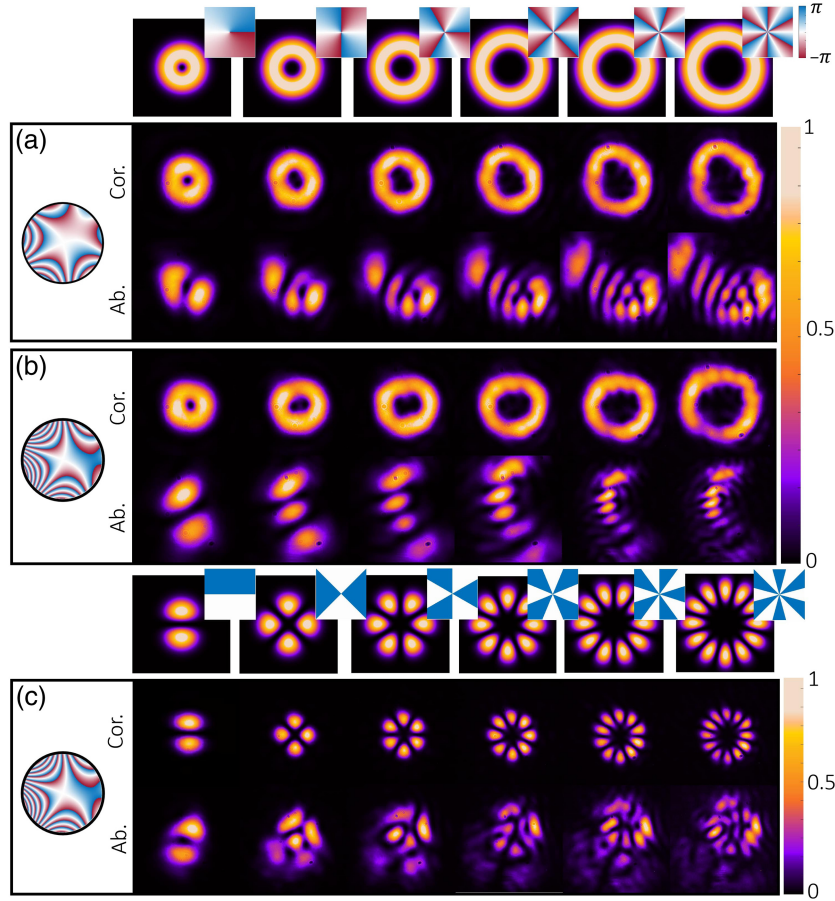


Fig. 4 Correction for superpositions of astigmatism and trefoil with arbitrarily chosen strengths. Left column insets show the aberrating phases acting on spatial modes (top insets). Experimentally aberrated (Ab.) and corrected (Cor.) far-field intensities for LG beams increasing columnwise in OAM from $\ell \in [1, 6]$ are given for aberrations with (a) three- and (b) four-mode superpositions. (c) Experimental results with the same OAM range for the LG superpositions $(\frac{1}{\sqrt{2}}(\text{LG}_\ell + \text{LG}_{-\ell}))$ are given for the same four-mode aberration.

the primary (major) aberration in any system of interest. As an example, phase insets (dispersive aberrations) show astigmatism aberrations incurred by wavelengths that have a factor of $\alpha = 2$ difference between them. By splitting, resizing, and recombining the aberrated beams correctly, a perfect corrective overlap is formed in the crystal (insets above NLC show the overlapped phases) as part of the nonlinear detection system. Alternatively, one can use a two-step nonlinear adjustment such that the probe is with the same wavelength as the signal and thus incurs identical distortions, as illustrated in Fig. 5(b). On the detection side, the aberrated probe is shifted to a desired wavelength for DFG while retaining the aberration by using another unstructured pump. The new probe is then recombined with the signal using a DM for the DFG process in a second crystal.

We now experimentally verify that resizing the beam, as shown in Fig. 5(a), correctly compensates for the difference in aberrational strength. To do so, a mismatch of $\beta = \frac{w_2}{w_1} = 1.4663$ between the probe (w_2) and signal (w_1) beam waists was made when demagnified onto the crystal in Fig. 1. The encoded phase gradient of each aberration (i.e., strength) was then altered by changing the coefficient, C_j , of the phases (e.g., $\Phi_{\text{Ab}} = CZ_{n,m}$) imparted by the SLM of beam $j = \{1, 2\}$. Using the similarity

($S = \frac{[\sum_{x,y} \sqrt{I_{\text{NA}}(x,y)I_{\text{Cor}}(x,y)}]^2}{\sum_{x,y} I_{\text{NA}}(x,y) \sum_{x,y} I_{\text{Cor}}(x,y)}$) between the measured unaberrated ($I_{\text{NA}}(x, y)$) and probe-corrected ($I_{\text{Cor}}(x, y)$) DFG intensity distributions, we quantify the correction efficacy for a range of coefficient values (C_1) encoded on the probe, while the signal remained fixed. $S = 1$ ($S < 1$) indicates perfect correction (presence of uncorrected aberrations). For generality, three cases where the aberrational Zernike order, magnitude of the aberration on the signal and spatial mode were tested are shown in Fig. 6. In each case, we find the same coefficients do not cancel the distortion in the generated beam. More specifically, in Fig. 6(a), we find an astigmatic $\text{LG}_{\ell=1}$ signal beam with a coefficient of $C_2 = 10$ requires a coefficient of $C_1 = 20.8$ on the probe to cancel the distortion due to weakening of the relative strength from the beam enlargement. For qualitative comparison, insets (i), (ii) give the experimental unaberrated and aberrated DFG beams, along with the aberrating mode (iii). Insets inside the plot show the corrected beams. Next, both the aberration type (trefoil) and strength ($C_2 = 15$) were altered in Fig. 6(b), giving optimal correction with $C_1 = 43.9$ and in Fig. 6(c), an astigmatic $\text{LG}_{\ell=2}$ with the same strength as Fig. 6(a) needs approximately the same strength ($C_1 = 21.4$). As the radial

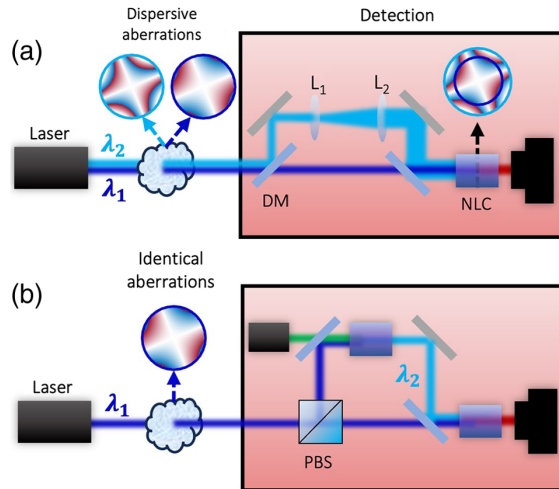


Fig. 5 Our approach can also be used in dispersive media. For instance, (a) by resizing the input beams of different wavelengths with experimental results shown in Fig. 6 and (b) by using the same initial wavelength in the dispersive media along with a second NLC for wavelength conversion prior to the DFG stage.

orders do not scale linearly with r but instead to its power, the relative strength changes as $\frac{C_2}{C_1} = \beta^m$ upon resizing. We find $\beta = 1.443, 1.431,$ and $1.466,$ respectively, from Fig. 6, which correlates well with the demagnification. Resizing the input modes relative to each other thus accurately compensates for the difference in phase due to dispersion. Using the factor $\alpha,$ the required corrective mismatch in beam size, $w_2 = w_1(\alpha)^{\frac{1}{m}} = w_1\left(\frac{\lambda_1 n_{\lambda_2}}{\lambda_2 n_{\lambda_1}}\right)^{\frac{1}{m}},$ can be calculated for any dispersive medium, where m is the main aberration order to be corrected. Note that if a second crystal is used, as shown in Fig. 5(b), then no size adjustment is needed nor is any prior knowledge of the aberration order.

Finally, we demonstrate a prepare-and-measure system that allows us to retrieve the correct encoded modes despite the presence of distortions. Here the conjugating nature allows not only the phase distortions to be eliminated, but the phase of equivalent spatial modes as well. For instance, only when the same OAM mode is encoded on the signal and probe does the DFG beam contain a flat phase. This forms a Gaussian intensity distribution in the far field that results in the presence of an on-axis intensity. Such matching of input modes (from the orthogonality relation of LG modes) allows it to also be used as a spatial mode detector. For continuity, we chose the same previous four-state Zernike superposition to be the aberration and show how such a detection system without aberration, with an aberrated signal beam and with a corrected detector mode (probe) performs. We do so in the case where the OAM beam modal profiles expand naturally with ℓ as well as when a mitigation of this expansion is encoded by a size-adjustment of $\frac{w}{\sqrt{(\ell+1)}}$ for each mode. In the first case, observation of the detection system for the ground truth (before aberrations) may be noted as having some higher-mode cross talk in the detection matrix [Fig. 7(a)], but largely detects the correct encoded OAM. However, with aberrational effects added to the signal, one is not able to distinguish the modes sent as seen with cross talk extending to adjacent modes and forming a cross-diagonal pattern. Applied

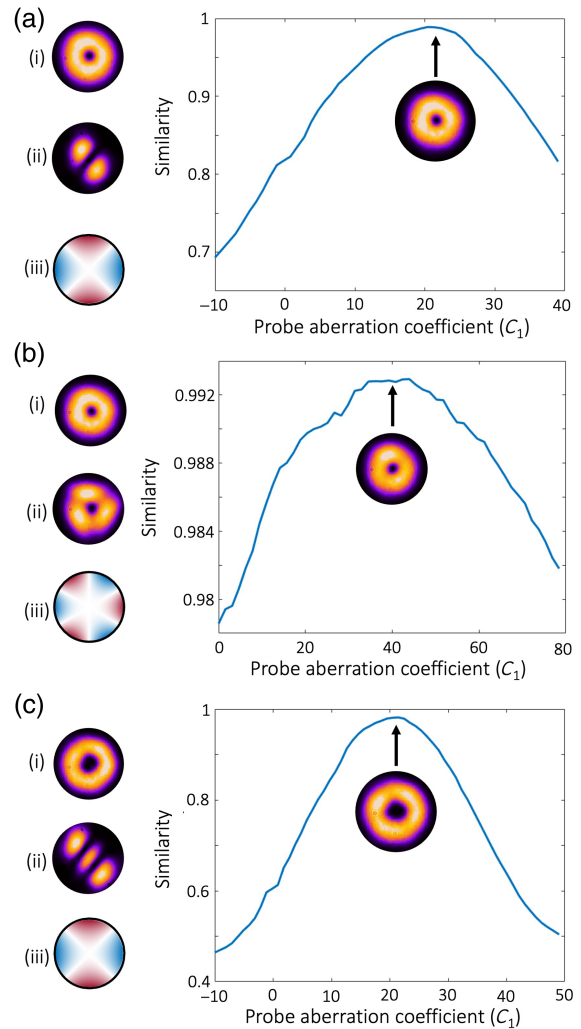


Fig. 6 Experimental results: resizing one beam changes the relative strength of the aberrations for (a) $\ell = 1$ with astigmatism ($m = 2$) and coefficient of 10 (measured $\beta = 1.443$), (b) $\ell = 1$ with trefoil ($m = 3$) and coefficient of 15 (measured $\beta = 1.431$), and (c) $\ell = 2$ with astigmatism ($m = 2$) and coefficient of 10 (measured $\beta = 1.466$). Leftmost insets show the (i) unaberrated downconverted mode, (ii) aberrated downconverted mode (no correction), and (iii) aberrating Zernike mode phase distribution.

corrections on the detection beam retrieve the detection diagonal, although it begins to degrade as the higher-order modes are used. This can be attributed to the enlarged sizes on both the detection and signal beams causing additional aberrations and mismatch being accumulated throughout the optical system for both the beams. This detracts from the encoded and corrected aberrations. Confirmation of this may be observed in the case where the expansion of the beams was mitigated in Figs. 7(d)–7(f), where the ground-truth detection matrix [Fig. 7(d)] already demonstrates an improvement in the system. The aberrational effects in Fig. 7(e) are additionally mitigated, but a clear distortion of the information being sent is still present, where adjacent modes are detected along with the modes being sent. Application of the correction on the detector mode then fixes the aberrational effects to yield the detection of the correct modes [Fig. 7(f)], in close agreement to what was observed for the nonaberrational case in Fig. 7(d).

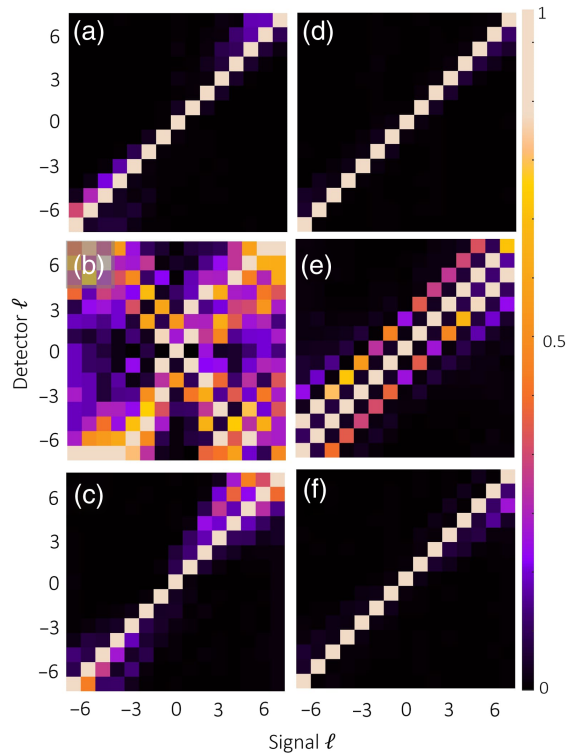


Fig. 7 Probe field is used as a detector for OAM modes of $\ell \in [-7, 7]$ in the cases where (a)–(c) the beam size expands as dictated by the OAM value and (d)–(f) a size adjustment of $\frac{w}{\sqrt{\ell+1}}$ is included to mitigate the OAM-dependent expansion in the generated modes. Detection cross talk matrices of the system are shown in (a) and (d) without applied aberrations; (b) and (e) with the four-mode Zernike aberration; and (c) and (f) with the aberrations corrected. Each row is normalized with the maximum value.

4 Discussion and Conclusion

Efficiency is always a concern in nonlinear experiments. In our experiment, with CW powers of 3.0 and 51 mW for the visible and IR light, respectively, we obtained approximate efficiencies ranging from $\approx 10^{-4}$ for $\ell = 1$ through to $\approx 10^{-5}$ for $\ell = 6$. However, this could be pushed up by orders of magnitude by optimized crystal parameters^{65–68} and pump shaping,⁶⁹ and holds unlimited potential with artificial resonant materials.^{70–73}

The limits of this technique relate to the interplay between efficiency, spatial resolution, and crystal parameters. For a given crystal size and length, there would be restrictions on the spatial resolution, where smaller transverse sizes act as an aperture to the incoming beams and thicker crystals limit both the spatial resolution of converted structure and, in the extreme cases, overall efficiency upon departing from the nondepletion regime. Naturally, one may circumvent this with larger and thinner crystals (reducing efficiencies), forming optimization parameters to engineer relating to the application requirements. Material availability also restricts the choice of wavelengths involved. In the event of dispersive aberrations, a compromise between efficiency and aberrational complexity dictates the suitable scheme for correction, as given in Fig. 6. Here correction restrained to a main order can be achieved without the need for a second nonlinear process, while removing the restriction on correction

complexity requires a reduction in efficiency with the addition of another nonlinear process. Of a more fundamental nature, both beams must overlap at the crystal for the process to work, and the beams should ideally be relayed (by a telescope, for instance) to the near field for optimal correction, so that some care must be taken in the optical arrangement.

To summarize, the practical implications of our measurement-free approach when different probes and signal wavelengths encounter a dispersive aberrating medium were considered and solutions explored. We showed that by resizing one input beam, it is possible to compensate for dispersion and thus correct the primary aberration, while using similar probe and signal wavelengths can reduce disparity at the cost of detecting DFG in the IR region. Full correction, however, is also ultimately possible using the same wavelengths and exploiting another nonlinear process for wavelength conversion before the corrective DFG process. Finally, by employing an identically aberrated detector beam, we were able to restore the ability to detect the encoded modes. Here good agreement was found between the detected and encoded modes that were left to scale in size with OAM charge and even further improvement when the scaling was compensated for. Such a system would be useful for retrieving information through noisy channels. Notably, the probing mechanism reliance on light itself renders it advantageous under rapidly varying distortions, such as atmospheric turbulence, making this technique a valuable tool for various applications, from optical communications to imaging and sensing. Furthermore, for a nondegenerate wavelength setup as used here, one is afforded the ability to detect in the VIS range when working with information carried by structured light in the difficult-to-detect NIR region.

In conclusion, we demonstrated the ability to use light as a method to correct aberrated modes through DFG, without the need for measurement. We have shown how this can be used in dispersive systems and demonstrated its efficacy with a prepare-and-measure communications protocol and with excellent signal recovery, even in the presence of a highly aberrated medium. Our approach offers a real-time measurement-free solution to undoing the action of a medium on structured light modes, with immediate applications in sensing, imaging, and communication.

5 Appendix

We can expand the concept and demonstrate that this correction is not exclusive to second-order nonlinear processes, but a general feature of parametric wave-mixing processes of even orders. In a general form, the nonlinear response of a medium to an incident field is of the form

$$\mathbf{P}^{(n+m)} = \chi^{(n+m)} \left(\prod_{i=1}^n \mathbf{E} \right) \left(\prod_{j=n+1}^{n+m} \mathbf{E}^* \right), \quad (3)$$

where $\mathbf{P}^{(n+m)}$ is the nonlinear polarization of the medium and $\chi^{(n+m)}$ is the susceptibility tensor.⁷⁴ The first and second products represent upconversion and downconversion processes, respectively, where the appropriate tensor components should be considered. Without loss of generality, any scalar component of an even nonlinear process involving input fields \mathbf{E}_1 and \mathbf{E}_2 can be written as

$$\mathbf{P}^{(2n)} = \chi^{(2n)} (\mathbf{E}_1 + \mathbf{E}_2)^n (\mathbf{E}_1^* + \mathbf{E}_2^*)^n. \quad (4)$$

Noticeably, there will be terms responsible for the excitation of fields with multiples of $\omega_G = \omega_1 - \omega_2$, which are the terms proportional to the powers of the product $E_1 E_2^*$. These are referred to as higher-order difference wave mixing⁷⁵ and represent the absorption of multiple photons at once. We can write them as

$$P^{(2n)}(n\omega_G) = \chi^{(2n)} M_1^n M_2^{n*} = A_1^n A_2^n e^{in(\Phi_1 - \Phi_2)}. \quad (5)$$

Similar to the initial argument, if $\Phi_1 = \Phi_{\text{info}} + \Phi_{\text{Ab}}$ and $\Phi_2 = \Phi_{\text{Ab}}$ then the generated phase profile would be $\Phi_G = n\Phi_{\text{info}}$. Additionally, by setting the absolute part A_2 to be spatially uniform, we see that the generated field $M_G^{(2n)} = M_1^n$, meaning that in this case the generated field is a positive integer power of the signal field. For the case of spatial transverse modes, such as LG and Hermite–Gaussian beams, these fields can be seen as multiple products of modes, for which there are one-to-one correspondences^{15,76,77} that essentially map the resulting field back to the original message unambiguously. In addition, this nonlinear dependence has been shown to be advantageous in detection processes.²⁵

As long as diffraction effects are negligible, this is true not only for a single process of DFG but also for cascaded nonlinear processes: every N_h 'th harmonic generation of E_1 would add an integer N_h multiple of the aberration profile to the phase profile—the same being true for E_2 in its N_k 'th harmonic. A number N_c of the cascaded DFG processes combines harmonics of E_1 and E_2 , thus applying a partial aberration correction N_c times. The total aberration correction is achieved when $N_h = (N_c - 1) + N_k$. It is important to notice that the combination of harmonics generation and DFG processes can be achieved in different media: instead of a single crystal or gas, it is possible to use a sequence of crystals or gas chambers combined by imaging systems. This can be used as method to optimize the efficiency of a certain process or enable specific wavelengths, which are not possible with a single process. This includes the case where a corrected beam is generated at the same wavelength as the original signal after two or more nonlinear interactions. In this case, a total depletion regime can be used for a complete substitution of the aberrated signal for a corrected beam.

Disclosures

The authors declare no conflicts of interest.

Code and Data Availability

Data underlying the results presented in this paper may be obtained from the authors upon reasonable request.

Acknowledgments

The authors would like to thank Dr. Isaac Nape and Dr. Paola Concha Obando for useful discussions. The authors acknowledge the funding from the Department of Science and Innovation as well as the National Research Foundation in South Africa. Support from the Italian Ministry of Research (MUR) through the PRIN 2017 project “Interacting photons in polariton circuits” (INPhoPOL) and the PNRR MUR project PE0000023-NQSTI is acknowledged. We also acknowledge support from the Italian Space Agency through the “High-dimensional quantum information” project.

References

1. A. Forbes, M. de Oliveira, and M. R. Dennis, “Structured light,” *Nat. Photonics* **15**, 253–262 (2021).
2. M. Wang et al., “Spin-orbit-locked hyperbolic polariton vortices carrying reconfigurable topological charges,” *eLight* **2**, 12 (2022).
3. C. He, Y. Shen, and A. Forbes, “Towards higher-dimensional structured light,” *Light: Sci. Appl.* **11**, 205 (2022).
4. Y. Yang et al., “Optical trapping with structured light: a review,” *Adv. Photonics* **3**, 034001 (2021).
5. A. E. Willner et al., “Orbital angular momentum of light for communications,” *Appl. Phys. Rev.* **8**, 041312 (2021).
6. G. Lazarev et al., “Beyond the display: phase-only liquid crystal on silicon devices and their applications in photonics,” *Opt. Express* **27**, 16206–16249 (2019).
7. A. Rubano et al., “Q-plate technology: a progress review,” *J. Opt. Soc. Am. B* **36**, D70–D87 (2019).
8. S. Scholes et al., “Structured light with digital micromirror devices: a guide to best practice,” *Opt. Eng.* **59**, 041202 (2020).
9. A. H. Dorrah and F. Capasso, “Tunable structured light with flat optics,” *Science* **376**, eabi6860 (2022).
10. C. Li et al., “Arbitrarily structured quantum emission with a multi-functional metalens,” *eLight* **3**, 19 (2023).
11. W. T. Buono and A. Forbes, “Nonlinear optics with structured light,” *Opto-Electron. Adv.* **5**, 210174 (2022).
12. H.-J. Wu et al., “Observation of anomalous orbital angular momentum transfer in parametric nonlinearity,” *Phys. Rev. Lett.* **130**, 153803 (2023).
13. Y. Chen et al., “Phase-matching controlled orbital angular momentum conversion in periodically poled crystals,” *Phys. Rev. Lett.* **125**, 143901 (2020).
14. Y. Tang et al., “Harmonic spin–orbit angular momentum cascade in nonlinear optical crystals,” *Nat. Photonics* **14**, 658–662 (2020).
15. H.-J. Wu et al., “Conformal frequency conversion for arbitrary vectorial structured light,” *Optica* **9**, 187–196 (2022).
16. M. Luttmann et al., “Nonlinear up-conversion of a polarization möbius strip with half-integer optical angular momentum,” *Sci. Adv.* **9**, eadf3486 (2023).
17. B. P. da Silva et al., “Observation of a triangular-lattice pattern in nonlinear wave mixing with optical vortices,” *Optica* **9**, 908–912 (2022).
18. N. R. da Silva et al., “Stimulated parametric down-conversion with vector vortex beams,” *Phys. Rev. Appl.* **15**, 024039 (2021).
19. S. Hancock et al., “Free-space propagation of spatiotemporal optical vortices,” *Optica* **6**, 1547–1553 (2019).
20. F. Steinlechner et al., “Frequency conversion of structured light,” *Sci. Rep.* **6**, 21390 (2016).
21. Z.-Y. Zhou et al., “Generation of light with controllable spatial patterns via the sum frequency in quasi-phase matching crystals,” *Sci. Rep.* **4**, 5650 (2014).
22. B. Sephton et al., “Spatial mode detection by frequency upconversion,” *Opt. Lett.* **44**, 586–589 (2019).
23. Y. Xu et al., “Orthogonal spatial coding with stimulated parametric down-conversion,” *Opt. Express* **31**, 42723–42729 (2023).
24. C. Schlickriede et al., “Nonlinear imaging with all-dielectric metasurfaces,” *Nano Lett.* **20**, 4370–4376 (2020).
25. X. Qiu et al., “Spiral phase contrast imaging in nonlinear optics: seeing phase objects using invisible illumination,” *Optica* **5**, 208–212 (2018).
26. P. S. Ribeiro et al., “Observation of image transfer and phase conjugation in stimulated down-conversion,” *Phys. Rev. Lett.* **87**, 133602 (2001).
27. A. V. Paterova et al., “Hyperspectral infrared microscopy with visible light,” *Sci. Adv.* **6**, eabd0460 (2020).
28. J. Rocha et al., “Speckle filtering through nonlinear wave mixing,” *Opt. Lett.* **46**, 3905–3908 (2021).

29. S. Trajtenberg-Mills, I. Juwiler, and A. Arie, "On-axis shaping of second-harmonic beams," *Laser Photonics Rev.* **9**, L40–L44 (2015).
30. E. Almeida, O. Bitton, and Y. Prior, "Nonlinear metamaterials for holography," *Nat. Commun.* **7**, 12533 (2016).
31. X. Fang et al., "High-dimensional orbital angular momentum multiplexing nonlinear holography," *Adv. Photonics* **3**, 015001 (2021).
32. X.-Y. Zhang et al., "Real-time superresolution interferometric measurement enabled by structured nonlinear optics," *Laser Photonics Rev.* **17**, 2200967 (2023).
33. B. Sephton et al., "Quantum transport of high-dimensional spatial information with a nonlinear detector," *Nat. Commun.* **14**, 8243 (2023).
34. X. Qiu, H. Guo, and L. Chen, "Remote transport of high-dimensional orbital angular momentum states and ghost images via spatial-mode-engineered frequency conversion," *Nat. Commun.* **14**, 8244 (2023).
35. D. Wei et al., "Experimental demonstration of a three-dimensional lithium niobate nonlinear photonic crystal," *Nat. Photonics* **12**, 596–600 (2018).
36. X. Xu et al., "Femtosecond laser writing of lithium niobate ferroelectric nanodomains," *Nature* **609**, 496–501 (2022).
37. Y. Zhang et al., "Nonlinear photonic crystals: from 2D to 3D," *Optica* **8**, 372–381 (2021).
38. Q. Guo et al., "Ultrathin quantum light source with van der Waals NbOCl₂ crystal," *Nature* **613**, 53–59 (2023).
39. O. Lib and Y. Bromberg, "Quantum light in complex media and its applications," *Nat. Phys.* **18**, 986–993 (2022).
40. S. Gigan et al., "Roadmap on wavefront shaping and deep imaging in complex media," *J. Phys.: Photonics* **4**, 042501 (2022).
41. S. Rotter and S. Gigan, "Light fields in complex media: mesoscopic scattering meets wave control," *Rev. Mod. Phys.* **89**, 015005 (2017).
42. H. Cao, A. P. Mosk, and S. Rotter, "Shaping the propagation of light in complex media," *Nat. Phys.* **18**, 994–1007 (2022).
43. A. G. de Oliveira et al., "Real-time phase conjugation of vector vortex beams," *ACS Photonics* **7**, 249–255 (2019).
44. R. A. Fisher, *Optical Phase Conjugation*, Academic Press (2012).
45. G. Sorelli et al., "Entanglement protection of high-dimensional states by adaptive optics," *New J. Phys.* **21**, 023003 (2019).
46. R. Grunwald et al., "High-flexibility control of structured light with combined adaptive optical systems," *Photonics* **9**, 42 (2022).
47. M. J. Booth, "Adaptive optical microscopy: the ongoing quest for a perfect image," *Light: Sci. Appl.* **3**, e165 (2014).
48. Y. Dai et al., "Active compensation of extrinsic polarization errors using adaptive optics," *Opt. Express* **27**, 35797–35810 (2019).
49. K. M. Hampson et al., "Adaptive optics for high-resolution imaging," *Nat. Rev. Methods Primers* **6**, 68 (2021).
50. Z. Cheng et al., "High-gain and high-speed wavefront shaping through scattering media," *Nat. Photonics* **17**, 299–305 (2023).
51. D. Bachmann et al., "Highly transmitting modes of light in dynamic atmospheric turbulence," *Phys. Rev. Lett.* **130**, 073801 (2023).
52. S. M. Popoff et al., "Measuring the transmission matrix in optics: an approach to the study and control of light propagation in disordered media," *Phys. Rev. Lett.* **104**, 100601 (2010).
53. I. M. Vellekoop and A. Mosk, "Universal optimal transmission of light through disordered materials," *Phys. Rev. Lett.* **101**, 120601 (2008).
54. A. Klug, C. Peters, and A. Forbes, "Robust structured light in atmospheric turbulence," *Adv. Photonics* **5**, 016006 (2023).
55. I. Nape et al., "Revealing the invariance of vectorial structured light in complex media," *Nat. Photonics* **16**, 538–546 (2022).
56. P. Pai et al., "Scattering invariant modes of light in complex media," *Nat. Photonics* **15**, 431–434 (2021).
57. W. Zhang et al., "Phase-matching in nonlinear optical compounds: a materials perspective," *Chem. Mater.* **29**, 2655–2668 (2017).
58. N. Bloembergen, "Conservation laws in nonlinear optics," *J. Opt. Soc. Am.* **70**, 1429–1436 (1980).
59. T. W. Clark et al., "Comparison of beam generation techniques using a phase only spatial light modulator," *Opt. Express* **24**, 6249–6264 (2016).
60. A. M. Yao and M. J. Padgett, "Orbital angular momentum: origins, behavior and applications," *Adv. Opt. Photonics* **3**, 161–204 (2011).
61. Y. Shen et al., "Optical vortices 30 years on: OAM manipulation from topological charge to multiple singularities," *Light: Sci. Appl.* **8**, 90 (2019).
62. V. Lakshminarayanan and A. Fleck, "Zernike polynomials: a guide," *J. Mod. Opt.* **58**, 545–561 (2011).
63. G. D. Love, "Wave-front correction and production of Zernike modes with a liquid-crystal spatial light modulator," *Appl. Opt.* **36**, 1517–1524 (1997).
64. J. Wang and D. E. Silva, "Wave-front interpretation with Zernike polynomials," *Appl. Opt.* **19**, 1510–1518 (1980).
65. W. Chen et al., "Continuous-wave mid-infrared laser sources based on difference frequency generation," *C. R. Phys.* **8**, 1129–1150 (2007).
66. M. Broyer et al., "Intracavity CW difference frequency generation by mixing three photons and using Gaussian laser beams," *J. Phys.* **46**, 523–533 (1985).
67. P. M. Vaughan and R. Trebino, "Optical-parametric-amplification imaging of complex objects," *Opt. Express* **19**, 8920–8929 (2011).
68. A. Barh et al., "Parametric upconversion imaging and its applications," *Adv. Opt. Photonics* **11**, 952–1019 (2019).
69. S. Singh et al., "Frequency conversion of orbital angular momentum with optimized efficiency and modal purity," *J. Opt. Soc. Am. B* **40**, 3128–3136 (2023).
70. L. Kang et al., "First-principles design and simulations promote the development of nonlinear optical crystals," *Acc. Chem. Res.* **53**, 209–217 (2019).
71. A. Autere et al., "Nonlinear optics with 2D layered materials," *Adv. Mater.* **30**, 1705963 (2018).
72. J. Chen et al., "High-performance second-harmonic-generation (SHG) materials: new developments and new strategies," *Acc. Chem. Res.* **54**, 2775–2783 (2021).
73. M.-Y. Li et al., "HgCuPS₄: an exceptional infrared nonlinear optical material with defect diamond-like structure," *Chem. Mater.* **32**, 4331–4339 (2020).
74. W. T. Buono et al., "Chiral relations and radial-angular coupling in nonlinear interactions of optical vortices," *Phys. Rev. A* **101**, 043821 (2020).
75. M. B. Gaarde, A. L'Huillier, and M. Lewenstein, "Theory of high-order sum and difference frequency mixing in a strong bichromatic laser field," *Phys. Rev. A* **54**, 4236 (1996).
76. V. V. Kotlyar et al., "Product of two Laguerre–Gaussian beams," *Photonics* **9**, 496 (2022).
77. G. Alves et al., "Conditions for optical parametric oscillation with a structured light pump," *Phys. Rev. A* **98**, 063825 (2018).

Sachleen Singh is a doctoral student at the Structured Light Laboratory at the University of the Witwatersrand, Johannesburg. Previously, he received his MSc in physics from the Indian Institute of Technology Ropar, India. He has prior experience in working with fibers and structured light. His present research aims to gain better control of quantum-structured light with nonlinear optics.

Berenice Sephton is a postdoctoral researcher in the Quantum Photonics Group at the University of Naples, Italy. She obtained her PhD in physics at the University of the Witwatersrand, South Africa, where she explored using nonlinear optics for quantum communication. Her current research interests span from structuring quantum states to exploiting structured light for imaging.

Biographies of the other authors are not available.